Beam Envelope Equations in a Solenoidal Field

G. Penn

UCB Physics / LBNL CBP

7 January 2000

MUON COLLIDER NOTE 71

Revision 1

Abstract

Ionization cooling of muons requires strong focussing of beams at the absorbers; solenoid magnets are required for cooling channels designed to use this mechanism. Assuming a cylindrically symmetric beam and using the single particle equations of motion, a set of transverse beam envelope equations are derived in the paraxial approximation. These equations incorporate the main factors in ionization cooling: interactions with material, acceleration by radio frequency (RF) cavities, and the possible accumulation of canonical angular momentum. The dominant nonlinear effect is the mirror force, which leads to estimates of beam correlation parameters for a matched beam. This formalism, analogous to the Courant-Snyder notation for systems of quadrupole lenses, allows for an analysis of lattice configurations beginning with thin lenses and then progressing to lattices of extended magnets. A categorization of lattice types connects this analysis with previous descriptions of cooling channels, including a "phase diagram" of lattice properties versus magnetic field profile. Scaling laws for channel performance are derived and exhibit good agreement with realistic lattice designs.

1. Introduction

In lattices designed for cooling of muon beams, the focussing will be accomplished through solenoidal magnets centered on the beam axis. A theoretical framework for understanding beam propagation and analysing lattice designs is built up and used to characterize some of the options for cooling channels. First, the single particle motion and appropriate betatron function in solenoid fields are described in a way that incorporates any canonical angular momentum carried by the beam. This formulation, adapted from the Courant-Snyder formalism for quadrupole focussing, offers a reliable correspondence in the paraxial approximation between lattices using solenoids and those using quadrupole magnets.

Equations for the single particle motion are obtained, and in the linear approximation constants of the motion are found. Proceeding to examine a simplified distribution of particles, a generalization of the beta function is described that allows for the case where net canonical angular momentum is carried by the beam. General scaling laws are given, as well as paraxial beam envelope equations incorporating energy loss in material, multiple scatter, and radio frequency (RF) acceleration.

Nonlinear effects are described, and they can cause significant growth in the rms emittance of a Gaussian beam. The coupling between longitudinal and transverse phase space is complicated, but mostly affects the forward momentum. In the transverse equations of motion, coupling only appears in third order corrections.

Idealized thin lens systems and then extended magnet geometries are examined, and used to put into context specific cooling channels which have been proposed previously. Furthermore, possibilities for new cooling channels are suggested by this analysis.

2. Single Particle Motion in a Solenoidal Field

We first consider single particle equations of motion in vacuum with magnetic fields only, and incorporate nonlinear effects. The magnetic field inside of a cylindrically symmetric solenoid is given by

$$\vec{B} = -\frac{\partial \mathcal{A}_\phi}{\partial z}\hat{e}_r + \frac{1}{r}\frac{\partial}{\partial r}(r\mathcal{A}_\phi)\hat{e}_z,$$

where $\mathcal{A}_\phi(r,z)$ satisfies

$$\frac{\partial^2 \mathcal{A}_\phi}{\partial z^2} + \frac{\partial}{\partial r}\left[\frac{1}{r}\frac{\partial}{\partial r}(r\mathcal{A}_\phi)\right] = 0.$$

Expanding in radius, we find

$$\mathcal{A}_\phi \simeq \frac{r}{2}B(z) - \frac{r^3}{16}B''(z) + \mathcal{O}\left(r^5\right),$$

where $B(z) \equiv B_z(r=0,z)$. The equations of motion are

$$P_z P_z' = q\frac{1}{r}\frac{\partial \mathcal{A}_\phi}{\partial z}(xP_y - yP_x)$$

$$P_z P_x' = q\frac{1}{r}\frac{\partial \mathcal{A}_\phi}{\partial z}P_z y + q\frac{1}{r}\frac{\partial}{\partial r}(r\mathcal{A}_\phi)P_y$$

$$P_z P_y' = -q\frac{1}{r}\frac{\partial \mathcal{A}_\phi}{\partial z}P_z x - q\frac{1}{r}\frac{\partial}{\partial r}(r\mathcal{A}_\phi)P_x.$$

Also, $x' = P_x/P_z$ and $y' = P_y/P_z$. The constants of motion are P^2 (equivalently, energy) and the canonical angular momentum,

$$L_{\rm canon} = xP_y - yP_x + qr\mathcal{A}_\phi.$$

We can simplify these expressions if we consider a rotating coordinate frame (the Larmor frame). Thus, using rotated coordinates

$$X_R = x\cos\varphi - y\sin\varphi, \qquad Y_R = x\sin\varphi + y\cos\varphi,$$

and defining $\varphi' = \kappa$, we have

$$X_R' = x'\cos\varphi - y'\sin\varphi - \kappa Y_R$$

$$Y_R' = y'\cos\varphi + x'\sin\varphi + \kappa X_R.$$

Consider the quantity

$$P_z(X_R Y_R' - Y_R X_R') = P_z\left(xy' - yx' + \kappa r^2\right);$$

this is equal to the canonical angular momentum if we set

$$\kappa = \frac{q\mathcal{A}_\phi}{P_z r} \simeq \frac{qB(z)}{2P_z}.$$

Note that as here defined $\kappa(r,z)$ depends on transverse position, but to lowest order is proportional to $B(z)/P_z$.

The equations of motion in terms of these rotating coordinates can be simplified to

$$X_R'' = -\kappa^2 X_R + \frac{q}{P_z}\left[X_R\frac{1}{r}\frac{\partial}{\partial r}\left(\frac{\mathcal{A}_\phi}{r}\right) - X_R'\frac{\partial}{\partial z}\left(\frac{\mathcal{A}_\phi}{r}\right)\right]\left[X_R Y_R' - Y_R X_R' - \kappa(X_R^2 + Y_R^2)\right]$$

$$Y_R'' = -\kappa^2 Y_R + \frac{q}{P_z}\left[Y_R\frac{1}{r}\frac{\partial}{\partial r}\left(\frac{\mathcal{A}_\phi}{r}\right) - Y^{c\prime}\frac{\partial}{\partial z}\left(\frac{\mathcal{A}_\phi}{r}\right)\right]\left[X_R Y_R' - Y_R X_R' - \kappa(X_R^2 + Y_R^2)\right].$$

Linearly, this is just

$$X_R'' = -\left(\frac{qB(z)}{2P_z}\right)^2 X_R, \tag{1}$$

and similarly for Y_R, with nonlinear terms only appearing to third order.

The longitudinal dynamics, which in vacuum only has nonlinear terms related to the mirror force, is given by

$$P_z' = q\frac{\partial}{\partial z}\left(\frac{\mathcal{A}_\phi}{r}\right)\left[X_R Y_R' - Y_R X_R' - \frac{qr\mathcal{A}_\phi}{P_z}\right].$$

Thus, we can solve linearly for transverse coordinates, then obtain the second order evolution of P_z, and use this to find the transverse corrections to third order.

We can define a betatron function and phase by

$$\Phi' = \frac{1}{\beta_p},$$

$$2\beta_p\beta_p'' - (\beta_p')^2 + 4\beta_p^2\kappa^2 - 4 = 0,$$

where $\kappa^2(z) = (qB(z)/2P_z)^2$ is the linearized focussing term. In contrast with quadrupoles, the focussing strength is always positive in both transverse directions. Then the linear solution in rotated coordinates is

$$X_R = A_1\sqrt{\beta_p}\cos(\Phi - \Phi_1)$$

$$Y_R = A_2\sqrt{\beta_p}\cos(\Phi - \Phi_2),$$

or in the lab frame

$$x = \sqrt{\beta_p}\left[A_1\cos\varphi\cos(\Phi - \Phi_1) + A_2\sin\varphi\cos(\Phi - \Phi_2)\right]$$

$$y = \sqrt{\beta_p}\left[-A_1\sin\varphi\cos(\Phi - \Phi_1) + A_2\cos\varphi\cos(\Phi - \Phi_2)\right].$$

To this order, there are two additional constants of the motion, the transverse amplitudes A_1 and A_2 which correspond to the Courant-Snyder invariants. Note that the focussing looks similar to that of a quadrupole only in the rotating coordinate frame. In terms of these amplitudes, the angular momentum is

$$L_{\rm canon} \simeq P_z A_1 A_2 \sin(\Phi_2 - \Phi_1). \tag{2}$$

The forward momentum satisfies

$$\left(P_z^2 - \frac{2}{r}q\mathcal{A}_\phi L_{\rm canon}\right)' = -r^2\left(\frac{q^2\mathcal{A}_\phi^2}{r^2}\right)' - \frac{2P_r}{P_z}\frac{\partial}{\partial r}\left(\frac{q\mathcal{A}_\phi}{r}\right)(xP_y - yP_x).$$

Using conservation of total momentum and defining $P_\perp^2 \equiv P_x^2 + P_y^2$, this can be expressed in terms of the magnetic moment:

$$\left(\frac{rP_\perp^2}{2\mathcal{A}_\phi}\right)' = \left(\frac{r}{\mathcal{A}_\phi}\right)'\left[\frac{1}{2}P_\perp^2 + \frac{q\mathcal{A}_\phi}{r}(xP_y - yP_x)\right] + \frac{1}{P_z\mathcal{A}_\phi}\frac{\partial}{\partial r}\left(\frac{q\mathcal{A}_\phi}{r}\right)(xP_x + yP_y)(xP_y - yP_x).$$

For a slowly varying magnetic field (compared to the betatron period), with $\beta_p \approx 1/\kappa$, the lowest order term reduces to

$$\left(\frac{P_\perp^2}{B}\right)' \simeq P_z^2\kappa'\left[A_1^2\cos 2(\Phi - \Phi_1) + A_2^2\cos 2(\Phi - \Phi_2)\right],$$

which averages to zero over a betatron period. However, because the solenoidal field and betatron phase can have similar length scales, the nature of the second order correction is in

general complicated and depends on the particulars of the magnetic geometry. The evolution of the longitudinal momentum remains consistent with

$$P_z^2 \left[1 + (x')^2 + (y')^2\right] = P^2,$$

which is simpler because the transverse motion is more weakly affected by the longitudinal-transverse coupling.

3. Linearized Envelope Equations

Above we examined individual particle trajectories; now we consider a simplified distribution in transverse phase space, which is 4-dimensional because of the coupling between x and y co-ordinates. For a cylindrically symmetric beam, the distribution should in general be a function of the angular momentum $L_{\rm canon}$ and the combined amplitude $A_1^2 + A_2^2$. In the lab frame, this combined amplitude can be expressed as

$$A_1^2 + A_2^2 = \gamma_p(x^2 + y^2) + \beta_p[(x')^2 + (y')^2] + 2\alpha_p(xx' + yy') + 2\beta_p\kappa(xy' - yx').$$

Here,

$$\gamma_p \equiv \frac{1}{\beta_p}(1 + \alpha_p^2 + \beta_p^2\kappa^2),$$

$$\beta_p' = -2\alpha_p,$$

and

$$\alpha_p' = 2\beta_p\kappa^2 - \gamma_p.$$

Because we are using rotating co-ordinates, the above expressions are different than those of a quadrupole, where $\gamma = (1 + \alpha^2)/\beta$ and there are no cross terms in the amplitude.

To obtain a set of simple expressions for the envelope equation, we consider a one-parameter family of functions of $A_1^2 + A_2^2$ and $L_{\rm canon}$. A convenient choice is a linear combination of the two terms,

$$A_\perp^2 \equiv \sqrt{1 + \mathcal{L}^2}(A_1^2 + A_2^2) - 2\mathcal{L}\frac{L_{\rm canon}}{P_z}, \tag{3}$$

where $\mathcal{L}$ is a dimensionless parameter indicating the net canonical momentum of the beam. This is the only way to incorporate canonical momentum and still have a simple Gaussian distribution. The particular form chosen for the combination of terms guarantees that $A_\perp^2$ is always positive. A Gaussian beam will then have a distribution function given by

$$F = \frac{NP_z^2}{4\pi^2 m^2 c^2 \epsilon_N^2} \exp\left(-\frac{P_z A_\perp^2}{2mc\epsilon_N}\right), \tag{4}$$

where $\epsilon_N = (P_z/mc)\langle A_\perp^2\rangle/4$ is the normalized transverse emittance; note that the term in the exponential is composed solely of second order quantities.

Expanding this total amplitude,

$$A_\perp^2 = \frac{1}{\beta_\perp}\left(x^2+y^2\right) + \beta_\perp\left(\frac{\mathcal{P}_x}{P_z} + \frac{\alpha_\perp}{\beta_\perp}x + \frac{\mathcal{L}}{\beta_\perp}y\right)^2 + \beta_\perp\left(\frac{\mathcal{P}_y}{P_z} + \frac{\alpha_\perp}{\beta_\perp}y - \frac{\mathcal{L}}{\beta_\perp}x\right)^2,$$

where

$$\mathcal{P}_x = P_x - q\frac{\mathcal{A}_\phi}{r}y \qquad \text{and} \qquad \mathcal{P}_y = P_y + q\frac{\mathcal{A}_\phi}{r}x$$

are the canonical momenta, and

$$\beta_\perp = \beta_p\sqrt{1+\mathcal{L}^2}, \qquad \alpha_\perp = \alpha_p\sqrt{1+\mathcal{L}^2}.$$

We will see below that

$$\mathcal{L} \simeq \frac{\langle L_{\rm canon}\rangle}{2mc\epsilon_N}.$$

Note that there is a single beta function $\beta_\perp(z)$ describing a cylindrically symmetric beam, and that this is not in general the same as the single-particle function $\beta_p(z)$. From this point of view, the actual choice of initial $\beta_\perp$, $\alpha_\perp$, and $\mathcal{L}$ corresponds to the initial shape of the beam envelope. It is the distribution as a whole which characterizes these parameters.

Linearly,

$$\mathcal{A}_\phi(r,z) \simeq \frac{r}{2}B_z(r=0,z) \tag{5}$$

and

$$\kappa(z) \simeq \frac{qB_z(r=0,z)}{2P_z} \simeq 0.15\frac{B[\mathrm{T}]}{P_z[\mathrm{GeV/c}]}\mathrm{m}^{-1}. \tag{6}$$

Then the equations of motion simplify to

$$x'' \simeq -2\kappa y' - \kappa' y,$$

$$y'' \simeq 2\kappa x' + \kappa' x.$$

Also,

$$A_\perp^2 \simeq \frac{x^2+y^2}{\beta_\perp} + \beta_\perp\left(x' - \kappa y + \frac{\mathcal{L}}{\beta_\perp}y + \frac{\alpha_\perp}{\beta_\perp}x\right)^2 + \beta_\perp\left(y' + \kappa x - \frac{\mathcal{L}}{\beta_\perp}x + \frac{\alpha_\perp}{\beta_\perp}y\right)^2.$$

The (symmetric) transverse moments matrix M for the Gaussian beam distribution given by Eq. (4) is

	x	P_x	y	P_y
x	$\epsilon_N\beta_\perp mc/P_z$			
P_x	$-mc\epsilon_N\alpha_\perp$	$mcP_z\epsilon_N\gamma_\perp$		
y	0	$mc\epsilon_N(\beta_\perp\kappa - \mathcal{L})$	$\epsilon_N\beta_\perp mc/P_z$	
P_y	$-mc\epsilon_N(\beta_\perp\kappa - \mathcal{L})$	0	$-mc\epsilon_N\alpha_\perp$	$mcP_z\epsilon_N\gamma_\perp$

(7)

where

$$\gamma_\perp \equiv \frac{1}{\beta_\perp}\left[1 + \alpha_\perp^2 + (\beta_\perp\kappa - \mathcal{L})^2\right],$$

and ϵ_N is the normalized transverse emittance. Because of the cylindrical symmetry, the matrix M is also the covariance matrix; in addition, the determinant of M simplifies to

$$\det\ M = \left[\langle x^2\rangle\langle P_x^2\rangle - \langle xP_x\rangle^2 - \langle xP_y\rangle^2\right]^2.$$

The emittance satisfies the expected condition

$$\det\ M = m^4c^4\epsilon_N^4.$$

Some other useful moments of the beam are the average mechanical angular momentum,

$$\langle xP_y - yP_x\rangle = -2mc\epsilon_N(\beta_\perp\kappa - \mathcal{L}),$$

and the net canonical angular momentum,

$$\langle L_{\rm canon}\rangle \simeq 2mc\epsilon_N\mathcal{L}.$$

This result neglects nonlinear terms in the vector potential.

In a vacuum with only magnetic fields, the beam parameters evolve according to

$$\beta_\perp' = -2\alpha_\perp$$

and

$$\alpha_\perp' = 2\kappa(\beta_\perp\kappa - \mathcal{L}) - \gamma_\perp.$$

The parameters $\mathcal{L}$ and ϵ_N are constant. This yields the envelope equation

$$2\beta_\perp\beta_\perp'' - (\beta_\perp')^2 + 4\beta_\perp^2\kappa^2 - 4(1+\mathcal{L}^2) = 0, \tag{8}$$

which differs from the single particle case only through the term $1+\mathcal{L}^2$. Any solution to the single-particle beta function can be multiplied by $\sqrt{1+\mathcal{L}^2}$ to yield a similar solution for the beam envelope. Thus, canonical momentum always causes beams to have a larger spot size, even when there is no actual emittance growth. In previous treatments, such as by M. Reiser [1], the envelope equation in vacuum, where the emittance and $\mathcal{L}$ are constant, show the combined effect of these two terms in determining the beam spot size. However, the interpretation of describing angular momentum as providing an "effective" emittance turns out not to be a useful concept when considering ionization cooling, where the uncorrelated spread of velocities determines the effectiveness of cooling. It is more natural in this context to ascribe the increase in spot size of a beam with angular momentum to an increase in the beta function.

For a beam to be matched into a uniform solenoid, $\mathcal{L}^2 = \beta_\perp^2\kappa^2 - 1$, so the average mechanical angular momentum is

$$\langle xP_y - yP_x\rangle = -2mc\epsilon_N\left[\beta_\perp\kappa \pm \left(\beta_\perp^2\kappa^2 - 1\right)^{1/2}\right],$$

which always has the sign of $-qB_z$ and cannot be equal to zero. This illustrates the fact that beams are only confined by solenoids when they have mechanical angular momentum

with this orientation; if a beam is not focussed and expands, however, diamagnetic forces generate just such a rotation and the beam will begin to experience a focussing force. Thus, a beam in a uniform solenoid which starts out at a size $\langle x^2 \rangle = R_0^2 = mc\epsilon_N\beta_\perp/P_z$ and with no mechanical angular momentum will always undergo betatron oscillations. If the initial $\alpha_\perp = 0$, then the initial transverse velocity spread is $\langle P_x^2 \rangle = P_0^2 = mcP_z\epsilon_N/\beta_\perp$ and the parameter $\mathcal{L} = \beta_\perp\kappa$. Then the largest size of the beam inside this solenoid occurs after a distance $\pi P_z/qB$ and is given by

$$R_{\max}^2 = R_0^2 + \left(\frac{mc\epsilon_N}{P_z\kappa R_0}\right)^2 = R_0^2 + 2\langle\rho_L^2\rangle,$$

where $\rho_L \equiv P_\perp/qB$ is the Larmor radius of a single particle orbit. The point of maximum beam size corresponds to half of a Larmor oscillation, where every particle is displaced by $2\rho_L$ in a direction uncorrelated with its initial position. When the beam is properly rotating to be matched, this introduces a correlation which causes the average radius of the particles to be unaltered by the Larmor oscillations.

4. Dynamics of the Beam Envelope

The evolution of an especially simple beam distribution was considered above; this example provides a model for analysing more general beams, as well as for parametrizing simulation results. The moments matrix M for any cylindrically symmetric beam has four independent terms, and can always be expressed in the form of Eq. (7) by a suitable choice of ϵ_N, $\beta_\perp$, $\alpha_\perp$, and $\mathcal{L}$. In addition, the parameter P_z must be specified because of the form chosen for the beta function (rather than using $\beta_\perp/P_z$, for example). Thus we normalize to the average P_z, and define

$$\begin{aligned} m^4c^4\epsilon_N^4 &= \det M, \\ \mathcal{L} &= \frac{\langle L_{\rm canon}\rangle}{2mc\epsilon_N}, \\ \beta_\perp &= \frac{\langle x^2\rangle\ \langle P_z\rangle}{mc\epsilon_N}, \\ \alpha_\perp &= -\frac{\langle xP_x\rangle}{mc\epsilon_N}. \end{aligned} \tag{9}$$

With matter and RF acceleration, the transverse properties of the beam are still adequately defined by these four transverse parameters, so long as coupling to the longitudinal phase space is weak. In addition, we will define the average linear focussing force to be

$$\kappa \equiv \frac{qB_z(r=0,z)}{2\langle P_z\rangle}. \tag{10}$$

An important point is that for a general distribution, even one for which there is no net canonical angular momentum, the envelope beta function as defined here need not correspond to the single-particle beta function, and its inverse is not equal to the phase advance per

unit length. However, this is still an informative way of parametrizing a beam, and for any particular beam distribution these quantities can be expressed in terms of the single particle beta function, for example by considering perturbations around Eq. (4).

The equations of motion for the beam envelope parameters, now redefined in terms of the lowest-order beam moments, can be derived by first neglecting multiple scattering and straggling, and assuming purely deterministic motion. Then an individual particle satisfies

$$x' = \frac{P_x}{P_z}, \qquad y' = \frac{P_y}{P_z},$$

and

$$v_z \frac{d\vec{P}}{dz} = \frac{d\vec{P}}{dt} = q(\vec{E} + \vec{v} \times \vec{B}) + \frac{\vec{P}}{P}\frac{dE}{ds}. \tag{11}$$

This implies that

$$P_z' \simeq \frac{qE_z}{v_z} + \frac{1}{v}\frac{dE}{ds} + \frac{q}{P_z}(P_x B_y - P_y B_x).$$

In the first-order results below, the term $P_x B_y - P_y B_x$ will be neglected because it is nonlinear, being related to the mirror force. Note that dE/ds, the energy change caused by material, is here defined as a negative quantity.

The averaging over particles which is performed when taking moments can be interchanged with the derivative, so that for example

$$\frac{d}{dz}\langle x^2 \rangle = \langle 2x\frac{P_x}{P_z} \rangle.$$

This yields an independent equation for each of the four independent terms of the moments matrix, and allows us to determine the dynamic equations of the four beam envelope parameters. Moments such as $\langle xE_x \rangle$ are set to zero, but they could be evaluated by a rudimentary space-charge model. These equations do couple to higher-order moments, however, leading to a hierarchy of moment equations. Here, we neglect nonlinear terms and coupling to longitudinal motion.

First, we add the effect of multiple scatter to this formalism. The spread in angles caused by multiple scatter is given by

$$\mathcal{D} \equiv \frac{d}{ds}\langle x'^2 \rangle \simeq \left(\frac{15 \text{ MeV}}{Pv}\right)^2 \frac{1}{L_R}, \tag{12}$$

using the Rossi-Greisen model [2] which fits a Gaussian to the Moliere model of multiple scatter. Multiple scatter adds a quantity $P_z P\mathcal{D}$ to the rate of change in $\langle P_x^2 \rangle$ and $\langle P_y^2 \rangle$, leaving all other moments unchanged. If we assume the beam remains cylindrically symmetric, then we can consider the beam envelope parameters to be defined by the beam moments as in Eq. (9).

In the limit where transverse fields are linear with radius and there is no coupling to longitudinal motion, the dynamic equations for the beam envelope are:

$$\epsilon_N' = \beta_\perp \frac{P\mathcal{D}}{2mc} + \epsilon_N \frac{1}{vP_z}\frac{dE}{ds}$$

$$
\begin{aligned}
\beta_\perp' &= -2\alpha_\perp + \beta_\perp \frac{qE_z}{v_z P_z} + \frac{\beta_\perp^2}{\epsilon_N}\frac{P\mathcal{D}}{2mc} \\
\alpha_\perp' &= -\gamma_\perp + 2\kappa(\beta_\perp \kappa - \mathcal{L}) - \frac{\alpha_\perp \beta_\perp}{\epsilon_N}\frac{P\mathcal{D}}{2mc} \\
\mathcal{L}' &= -\beta_\perp \kappa \frac{1}{vP_z}\frac{dE}{ds} - \frac{\mathcal{L}\beta_\perp}{\epsilon_N}\frac{P\mathcal{D}}{2mc}.
\end{aligned} \tag{13}
$$

Combined with the equation for P_z, these coupled equations determine the evolution of the beam. An approximate form for the momentum equation including mirror forces is

$$
\langle P_z \rangle' \simeq \frac{qE_z}{v_z} + \frac{1}{v}\frac{dE}{ds} - 2mc\epsilon_N \kappa'(\beta_\perp \kappa - \mathcal{L}). \tag{14}
$$

When the electric field is rapidly varying in time, an average of the field as seen by the particles at a given location must be taken as well.

Among the possible extensions of this paraxial theory are the inclusion of beam asymmetries, bending magnets, coupling to longitudinal phase space, nonlinear fields, space charge, and emittance growth. For example, the emittance growth in the absence of material or applied electric fields can be expressed as:

$$
\begin{aligned}
m^2c^2\epsilon_N\epsilon_N' &= \left\langle \frac{xP_x}{P_z} \right\rangle \left\langle P_x^2 \right\rangle - \langle xP_x \rangle \left\langle \frac{P_x^2}{P_z} \right\rangle \\
&\quad + \langle xP_y \rangle \left\langle \frac{qB_z}{P_z} xP_x \right\rangle - \left\langle \frac{qB_z}{P_z} xP_y \right\rangle \langle xP_x \rangle \\
&\quad + \left\langle x^2 \right\rangle \left\langle P_x \left(\frac{qE_x}{v_z} - qB_y \right) \right\rangle - \left\langle x \left(\frac{qE_x}{v_z} - qB_y \right) \right\rangle \langle xP_x \rangle \\
&\quad + \left\langle x \left(\frac{qE_y}{v_z} + qB_x \right) \right\rangle \langle yP_x \rangle .
\end{aligned} \tag{15}
$$

The above result assumes cylindrical symmetry. With specified external fields or a suitable model for space charge effects, the emittance growth can then be described in terms of a coupling to higher-order beam moments.

5. Comparison with Quadrupoles: Thin Lens Approximation

Because quadrupole lattices are often calculated using a thin lens approximation, we first consider a similar limit for lattices using solenoid focussing for the sake of comparison. We treat bi-periodic systems, which are particularly useful as models of the solenoid geometries being considered in Section 8.

We have found an equation for the cylindrical beta function, Eq. (8),

$$
2\beta_\perp \beta_\perp'' - (\beta_\perp')^2 + 4\beta_\perp^2 \kappa^2 - 4(1 + \mathcal{L}^2) = 0.
$$

This is identical to the equation for a focussing quadrupole in one dimension except for the scaling factor $\beta_\perp \propto (1 + \mathcal{L}^2)^{1/2}$, if we identify κ^2 with the quadrupole focussing intensity $|qB'/P_z|$. The focussing intensity for a solenoid is quadratic in B/P_z, however, which does

lead to different dynamics in terms of energy acceptance of a given lattice. For now we set $\mathcal{L} = 0$. We examine the properties of thin lens configurations to illustrate beam focussing in solenoidal channels.

We first consider a thin lens of length ℓ, which for a quadrupole has focal length f given by

$$\frac{1}{f_{\rm quad}} = \int dz \frac{qB'}{P_z} \simeq \frac{\ell q B'}{P_z}. \tag{16}$$

For a solenoid,

$$\frac{1}{f_{\rm s}} = \int dz \frac{q^2 B^2}{4P_z^2} \simeq \frac{\ell q^2 B^2}{4P_z^2}. \tag{17}$$

For a periodic lattice of solenoid lenses with periodicity L, it is useful to define the dimensionless parameter

$$\xi = \frac{L}{f} = L\ell\kappa^2. \tag{18}$$

Note that the sign of the magnetic field within each lens is irrelevant for this level of approximation, where the fringe fields from adjacent lenses do not overlap. Then for the simplest case of thin lenses spaced L apart, the acceptance of the lattice is given by $0 < \xi < 4$. We are going to perturb the lattice so that each periodic unit has two lenses, so we begin with lenses spaced by $L/2$. Because of this rescaling, the acceptance for ξ as defined above is

$$0 < \xi < 8.$$

Now, we perturb the lattice by shifting every other lens a fixed distance, so the periodicity is now L, and we define d as the shorter distance between lenses. We find that there is a new resonant region around $\xi = 4$ because there the betatron tune was $Q = 1/2$ (180 degree phase advance in a distance L, or 90 degree phase advance between lenses) in the unperturbed lattice. The geometry is shown in Figure 1. This defines two regions of momentum acceptance, Region I with

$$0 < \xi < \frac{2L}{L-d}$$

that accepts any momentum above some minimum value, and Region II with

$$\frac{2L}{d} < \xi < \frac{2L}{d} + \frac{2L}{L-d} = \frac{2L^2}{d(L-d)}.$$

Note that $d \leq L/2$. The transfer matrix over a distance L for the midpoint between the two closer lenses is

$$\begin{pmatrix} 1-\xi+d(L-d)\xi^2/(2L^2) & -(d\xi/2-L)\left[1-d(L-d)\xi/(2L^2)\right] \\ \left[(L-d)\xi-2L\right]\xi/L^2 & 1-\xi+d(L-d)\xi^2/(2L^2) \end{pmatrix} \tag{19}$$

The phase advance per cell is given by

$$\cos 2\pi Q = 1 - \xi + \frac{d}{2L^2}(L-d)\xi^2.$$

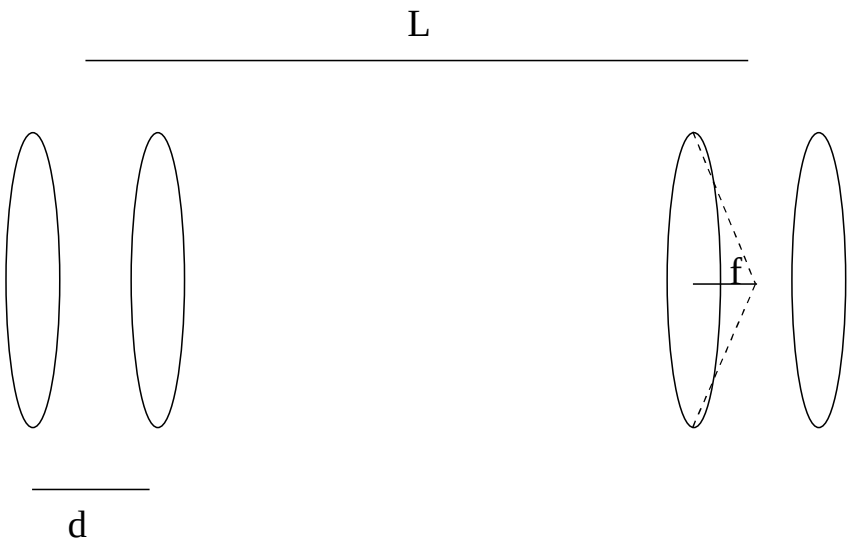

Figure 1: Thin lens geometry, with cell length L, coil separation d, and focal length f depicted.

Typical beta functions in Region I take their minimum value inside the larger gap between lenses, and the minimum beta function grows like $1/\xi$ as momentum gets large and $\xi \to 0$. Region II has a limited range of allowed momenta, and tends to have the minimum of the beta function occur in the smaller gap between lenses. Region II turns out to be the more interesting region for finding the lowest possible beta functions, because the minimum beta decreases as d/L decreases. This is true even if d is held fixed and L is increased, however this results in a smaller momentum acceptance. When operating the system of lenses at momenta corresponding to Region I, this benefit is not seen and the minimum $\beta_\perp$ is stuck with a scaling proportional to L.

In Region I, the minimum of the beta function is given by

$$\beta_1^2 = \frac{L^2}{2\xi}\left[1 - \frac{d(L-d)}{2L^2}\xi\right]\frac{2L-(L-d)\xi}{2L-d\xi}.$$

In Region II, the minimum of the beta function is given by

$$\beta_2^2 = \frac{L^2}{2\xi}\left[1 - \frac{d(L-d)}{2L^2}\xi\right]\frac{d\xi-2L}{(L-d)\xi-2L}.$$

In Region II, the minimum beta function goes to zero at the resonances which determine its momentum acceptance, and is largest (worst) close to the center of the momentum range, with value

$$\beta_{\rm M} = \frac{d^2}{L}\left(1+\sqrt{\frac{L-2d}{L}}\right)^{-2}.$$

We define the range $\Delta P/P$ of momentum acceptance as

$$P_0\left(1-\frac{\Delta P}{P}\right) < P_z < P_0\left(1+\frac{\Delta P}{P}\right);$$

for a quadrupole system

$$\frac{\Delta P}{P} = \frac{d}{2L - d},$$

while for a system of solenoids

$$\frac{\Delta P}{P} = \frac{d}{L}\left(1 + \sqrt{\frac{L-d}{L}}\right)^{-2},$$

which is roughly half the range as for a comparable quadrupole system because $\xi \propto 1/P_z^2$.

Roughly, for a given momentum acceptance, the furthest $\beta_\perp$ can be reduced is

$$\beta_\perp \simeq d\frac{\Delta P}{P} \simeq 4L\left(\frac{\Delta P}{P}\right)^2$$

so the main ways of reducing the beta function are taking down the momentum acceptance or pulling the lenses closer together, requiring stronger fields and current densities. The dependence of these quantities on the geometry of the lattice is illustrated with two figures, Figure 2 where the cell length is held fixed at 1 m, and Figure 3 where the coil separation d is held fixed at 25 cm. Data points found numerically using a moments code [3] are also indicated. We find good agreement except for the focal length. The expression

$$\frac{1}{f_{\rm s}} = \int ds \frac{q^2 B^2}{4P_z^2} \simeq \frac{\ell q^2 B^2}{4P_z^2}$$

consistently overestimates the strength of the lenses by about 15% because of their finite thickness, which was taken to be 1 cm compared to 10 cm for the focal length.

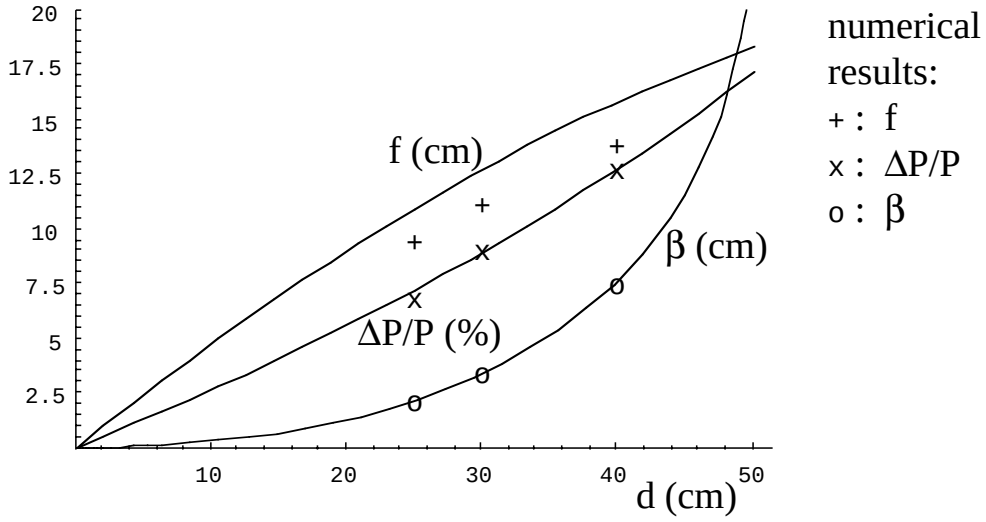

Figure 2: Lattice characteristics in thin lens geometry, with focal length f, momentum acceptance $\Delta P/P$, and minimum beta function β shown. Fixed cell length $L = 1$ m, and varying the coil separation, d.

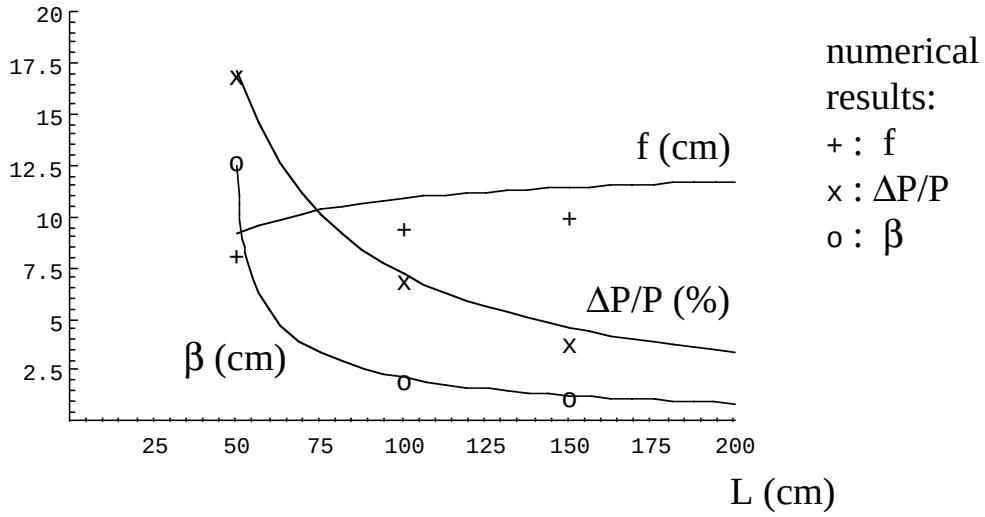

Figure 3: Lattice characteristics in thin lens geometry, with focal length f, momentum acceptance $\Delta P/P$, and minimum beta function β shown. Fixed coil separation $d = 25$ cm, and varying the cell length, L.

6. Scaling Laws

We keep our attention on Region II, where significant advantages are to be had from changing the geometry by closing the gap within pairs of lenses. The focal length for lenses, and thus magnetic field strength for a given momentum, depends primarily on d, and only slightly changes as different trade-offs are made between momentum acceptance and low beta functions. Specifically, at the central momentum the focal length f falls in the range

$$0.36\ d\ \lesssim\ f < 0.5\ d,$$

where the smaller f corresponds to larger momentum acceptance. This is simply due to the fact that the focal point should be close to the minimum beta, which is a distance $d/2$ away from the lens, and must be a little more strongly focussed than this because the beam is expanding when it hits the lens.

The only place the magnetic field strength appears is in the term $\kappa \propto B/P_z$, so for identical lattices the magnetic field can be brought down by lowering the momentum of the beam, and the beta function will remain identical. From momentum acceptance considerations, however, the fractional momentum spread σ_P/P should be kept the same, which may mean using longer bunches.

The beta function also scales with the overall length of the cell. Note that shrinking the entire system does not allow one to take advantage of the fact that $\xi \propto B^2$ because realistically, one must also shrink the length ℓ of each lens. In fact, if one is prevented from shrinking the aperture of the solenoid by the size of the beam, shrinking the system may make less of an improvement in lattice performance than a simple scaling law would suggest. To reduce the magnetic fields needed, it should be easier to stretch out a given geometry, at the expense of larger beta functions, however.

On the other hand, if one is willing to trade momentum acceptance for a small beta function, the periodicity L can be lengthened for a fixed set of pairs of solenoids, and the beta function will roughly scale as $1/L$. A useful "quality factor" for the tradeoff between momentum acceptance and low minimum beta functions is given by

$$Q_c \equiv \frac{L}{\beta_{\rm M}} \left(\frac{\Delta P}{P}\right)^2 \tag{20}$$

where $\beta_{\rm M}$ is the minimum of the matched beta function evaluated at the central value for the momentum. For a thin lens this factor ranges from roughly 0.12 for equally spaced lenses to 0.25 for very close pairs of lenses.

7. FOFO Lattices Described in Terms of a Single Parameter

We now begin to consider channels with extended solenoids, as opposed to thin lens models. A particularly simple but useful model for real lattices is an axial field which varies sinusoidally with longitudinal position. This is typically referred to as a FOFO lattice. Here, the FOFO lattice is described and general scaling laws are given. The minimum beta function can be expressed in terms of the cell length and the distance of the central momentum from the resonant momentum.

The magnetic field on axis of a FOFO lattice roughly follows a sine curve. Here we define $B_{\max}$ to be the maximum of the magnetic field, and L to be the length of the cell, which is one half-period of the magnetic field. The magnetic field on axis for the idealized lattice is

$$B_z(z) = B_{\max} \sin\left(\frac{\pi z}{L}\right).$$

The zeroes of the magnetic field are uniformly separated by L. Then for a given momentum P_z, the behavior of the lattice can be described in terms of the single parameter

$$\chi \equiv \frac{B_{\max}[\mathrm{T}]\ L[\mathrm{m}]}{P_z[\mathrm{GeV/c}]}. \tag{21}$$

Another way to think of this parameter is to treat $1/\chi$ as a dimensionless scaling of the momentum. For a given χ, all lattice parameters are completely determined, with the length scale being set by the cell length L. An equivalent expression is

$$\chi \simeq 6.671\ \kappa_{\max} L,$$

where the numerical factor is equal to $2 \times 10^9/c[\mathrm{m/s}]$. The beta function equation given by Eq. (8) can be written in dimensionless form as

$$2b\ddot{b} - \dot{b}^2 + 0.09\ \chi^2 \left(\frac{B}{B_{\max}}\right)^2 b^2 - 4 = 0, \tag{22}$$

where $b \equiv (1+\mathcal{L}^2)^{-1/2}\beta_\perp/L$, and the derivative is with respect to s/L.

For the FOFO lattice, the resonant momentum occurs roughly when $\chi \simeq 23.9$. The usual region of interest is $\chi < 23.9$. There are isolated regions of stability beyond this value, which have a narrow range of momentum acceptance. For example, the first region of stability beyond this value of χ occurs in the range $39.5 < \chi < 57.1$, and loosely corresponds to the "alternating solenoid" lattice. In this case the minimum beta occurs at the maximum magnetic field. An example of the beta function, when $B_{\max} = 4.75$ T, $L = 2$ m, and $P_z = 200$ MeV/c, is shown below.

It is useful to consider a rough fit to the numerical solutions, although much progress has been made by R.C. Fernow in obtaining analytic solutions to single-particle dynamics [4]. The fits below are chosen in such a way that they are correct in the limit $\chi \ll 1$, and properly exhibit the resonant behavior. If P_z is the central momentum of the beam, then the

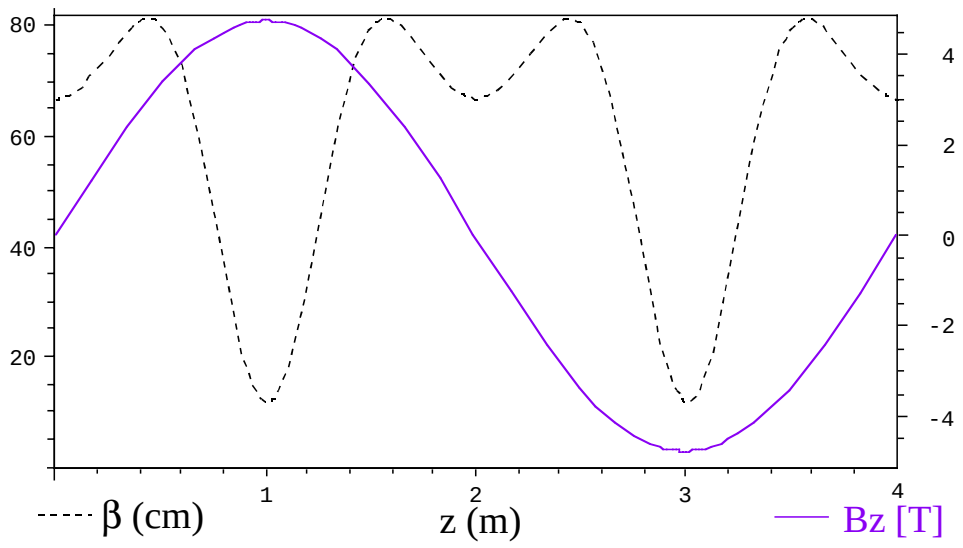

Figure 4: Analytic calculations of $\beta_\perp$ for a FOFO magnetic field when $B_{\max} = 4.75$ T, $L = 2$ m, and $P_z = 200$ MeV/c. This corresponds to the central momentum of the second region of stability, where the acceptance is $\pm 18\%$.

momentum acceptance is simply given by the resonant cutoff, $\chi \simeq 23.9$, so the maximum allowed deviation in momentum is

$$\frac{\Delta P}{P} \equiv \frac{P_z - P_{\rm cr}}{P_z} \simeq 1 - \frac{\chi}{23.9}.$$

For very low χ, the beam is very stiff and the beta function is roughly constant; the matching condition is determined by the average along the axis of the square of the magnetic field. The beta function is then given by $\beta_\perp \simeq 9.4\ L/\chi$, and the phase advance per cell is $\chi/9.4$. As χ increases, the beta function starts to vary along the cell and the phase advance per cell is larger than a linear extrapolation would indicate. In particular, a linear fit would predict resonance at $\chi \simeq 6.671\ \pi\sqrt{2} \simeq 29.6$, whereas the true resonance is estimated to occur near $\chi = 23.9$. In contrast, consider the thin lens approximation with a half cell replaced by a single lens having focal length

$$\frac{1}{f} = \int_0^L \kappa^2 dz = \frac{1}{2}\kappa_{\max}^2 L \simeq 0.0112\ \chi^2 \frac{1}{L}.$$

Then, the thin lens cutoff of $L/f = 4$ indicates a resonance occurring at $\chi = 18.9$, which is too low. This is another indication that the naive expression given by Eq. (17) underestimates the focal length of an extended lens. In addition, note that the higher order regions of stability do not appear as solutions of the thin lens model. We will find in Section 8 that the momentum acceptance of extended lens systems tends to be greater than a thin lens model would predict.

A better numerical fit for the phase advance per cell (again, half of a period in the

magnetic field) is, in degrees,

$$\Phi \simeq 180\frac{\chi}{23.9}\left\{1 - 0.19\left[1 - \left(\frac{\chi}{23.9}\right)^2\right]^{1/2}\right\}.$$

This has the correct resonance and in addition reduces to the appropriate limit for small χ. A phase advance of 90 degrees, where particle orbits are sensitive to small perturbations, occurs when $\chi \simeq 14.5$. Typically we want to restrict the beam to the range $14.5 < \chi < 23.9$.

A good fit for the minimum beta is

$$\beta_{\rm min} \simeq L\frac{9.4}{\chi}\left[1 - \left(\frac{\chi}{23.9}\right)^2\right]^{1/2}.$$

Close to resonance, this implies that the minimum beta scales as

$$\beta_{\rm min} \simeq 0.56\ L\left(\frac{\Delta P}{P}\right)^{1/2}.$$

The maximum beta is rougly

$$\beta_{\rm max} \simeq L\frac{9.4}{\chi}\left[1 - \left(\frac{\chi}{23.9}\right)^2\right]^{-1/2},$$

and becomes large very close to resonance. The aperture required to fit a given beam is determined by $\beta_{\rm max}$, which reaches a smallest value of $\approx 0.64\ L$ at $\chi \simeq 17$. However, there is little increase in $\beta_{\rm max}$ until about $\chi = 20$.

When considering beam correlations it is useful to know the quantity $\bar{\gamma_p}$, defined by

$$\bar{\gamma_p} \equiv \frac{1}{L}\oint \frac{dz}{\beta_p(z)}\left[1 + \left(\frac{\beta_p'(z)}{2}\right)^2 + \kappa^2(z)\beta_p^2(z)\right].$$

Here, L is the length of a cell, and the integration is taken over a single cell. The focussing strength along the lattice is

$$\kappa(z) = \frac{qB_z(z)}{2P_z}.$$

A close fit for $\bar{\gamma_p}$ (in FOFO lattices only) is

$$\bar{\gamma_p} \simeq \frac{2}{\beta_{\rm min}}\left[1 + \frac{1}{2}\left(\frac{\chi}{23.9}\right)^3\right]^{-1}.$$

Numerical results shown below were obtained in Mathematica using Eq. (22). Approximate fits are shown as dashed lines.

As a specific example, we consider $\chi = 18.0$, which corresponds to a momentum acceptance of about $\pm$ 24%. In Figure 9 we plot β_p/L and $1/(L\gamma_p)$ along the cell. In this case, $\beta_{\rm min} \simeq 0.35\ L$. Note that $1/\gamma_p$ varies in the opposite direction as the magnitude of the magnetic field.

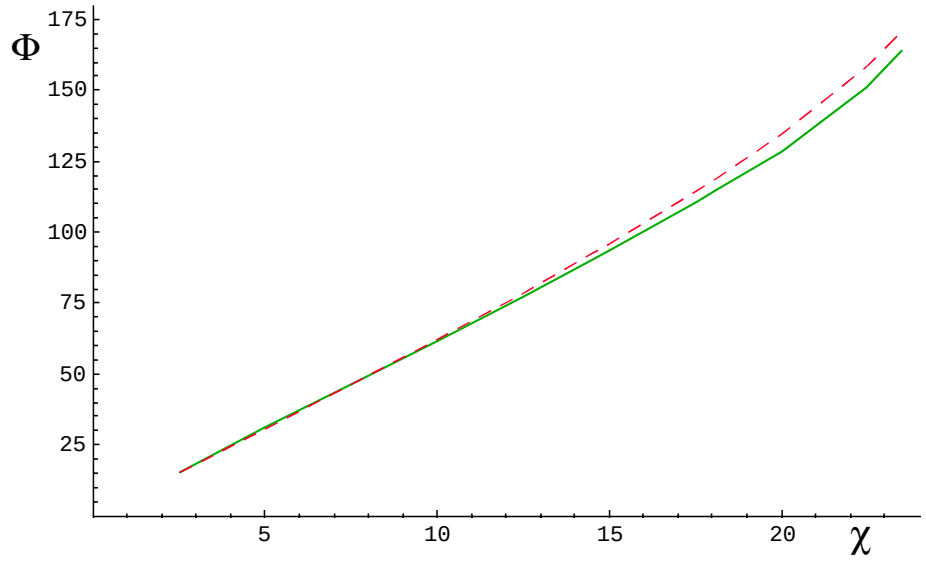

Figure 5: Analytic calculations of phase advance per cell (solid line), in degrees, along with numerical fit (dashed line).

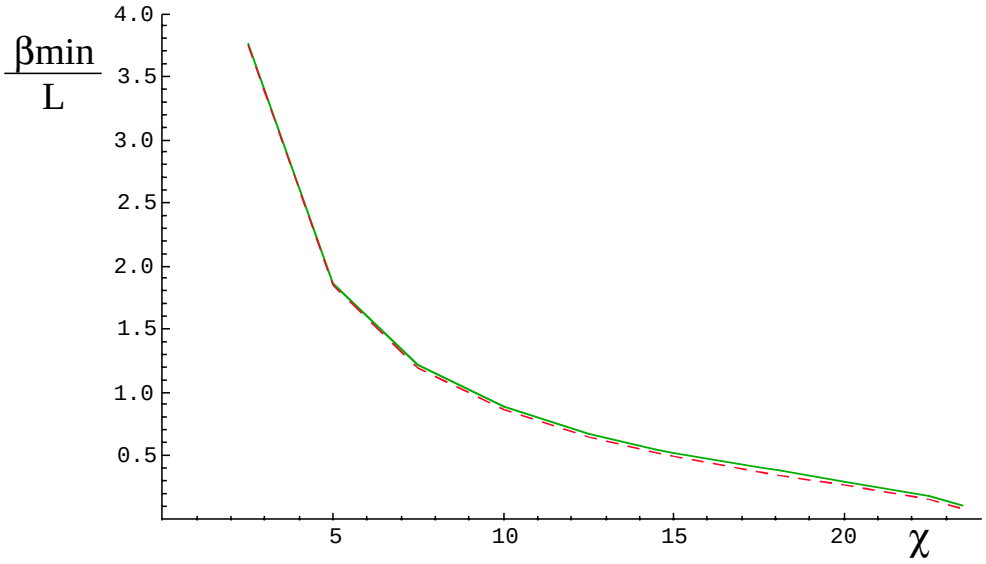

Figure 6: Analytic calculations of $\beta_{\min}/L$ (solid line) along with numerical fit (dashed line).

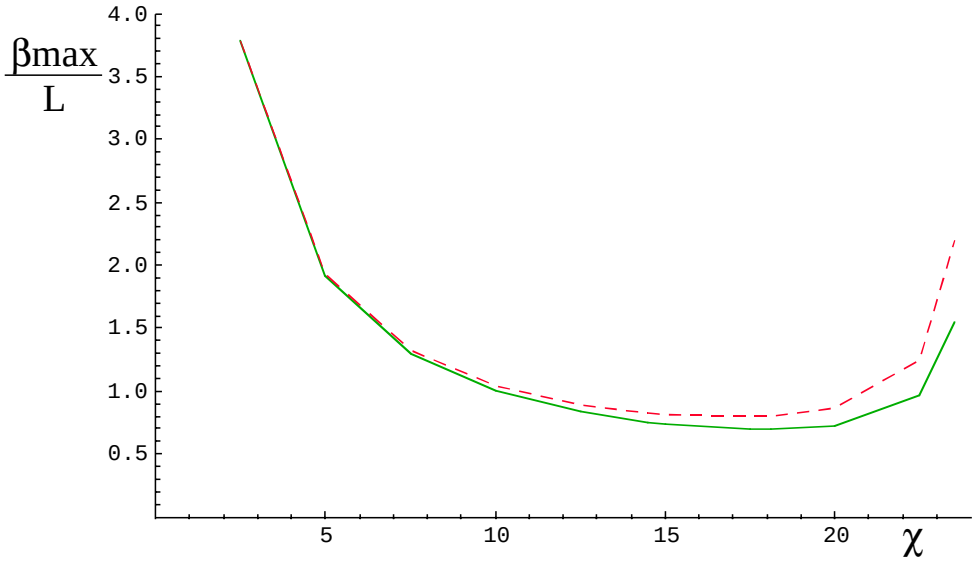

Figure 7: Analytic calculations of $\beta_{\max}/L$ (solid line) along with numerical fit (dashed line).

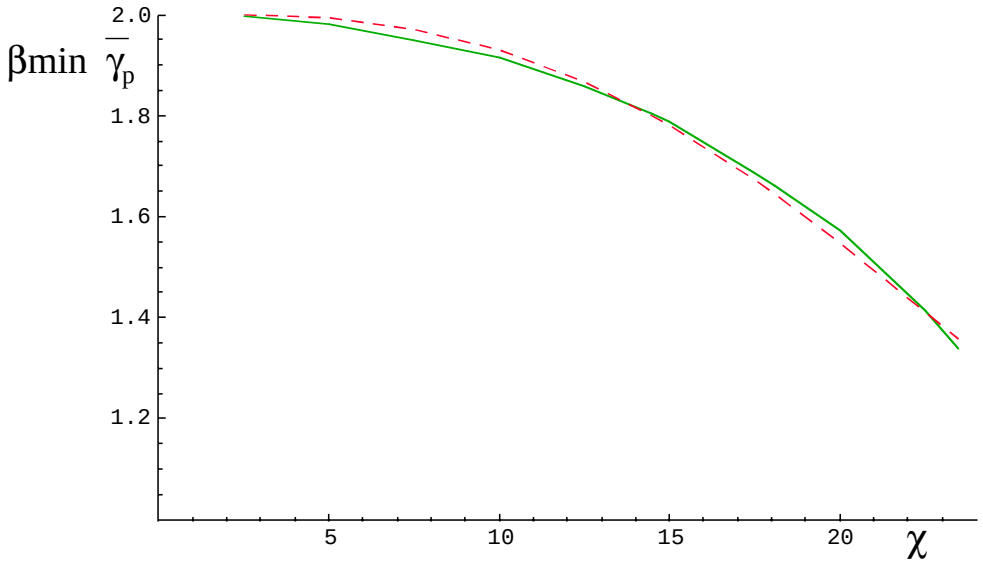

Figure 8: Analytic calculations of $\beta_{\min}\bar{\gamma}_p$ (solid line) along with numerical fit (dashed line).

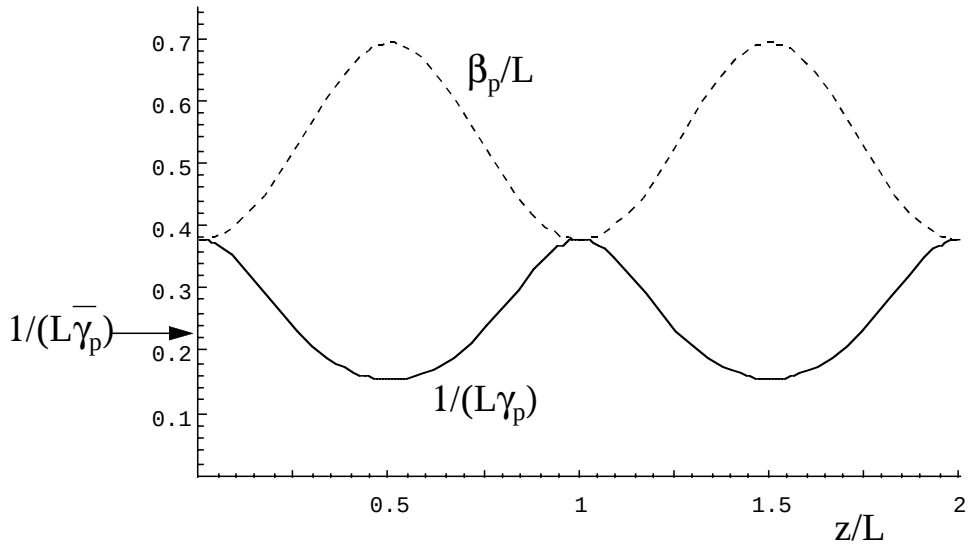

Figure 9: Analytic calculations of β_p/L (dashed line) and $1/(L\gamma_p)$ (solid line) for a FOFO cell with $\chi = 18.0$. The average value $L\bar{\gamma}_p$ is also indicated.

The acceptance of a FOFO channel has been examined in detail by R.C. Fernow [4], with analytic expressions for the transitions between bounded and unbounded particle motion. There is good agreement between these exact (in the paraxial approximation) results and the critical values of χ above, which were found by scanning the solutions to the dimensionless beta function equation. For comparison, it is useful to consider the evolution of the beam size, $R \propto \sqrt{\beta}$, which in a vacuum with no electric fields is determined by

$$R'' + \kappa^2 R - \frac{1}{R^3 P_z^2}\left[m^2 c^2 \epsilon_N^2 + \frac{1}{4}\langle L_{\rm canon}\rangle^2\right] = 0, \tag{23}$$

which is similar to the standard envelope equation for a charged particle beam except for the canonical momentum term from the factor $1 + \mathcal{L}^2$. In addition, the single particle equation of motion for the radius r is given by

$$r'' + \kappa^2 r - \frac{1}{r^3 P_z^2} L_{\rm canon}^2 = 0. \tag{24}$$

From either expression, the critical values of P_z can be found by neglecting the $1/r^3$ term and looking for unbounded solutions. The resulting simplified equation,

$$r'' + \kappa^2 r = 0, \tag{25}$$

becomes asymptotically close to the original equation as r becomes large. Thus, the cutoffs should agree. Another way to justify this is to restrict attention to particles with $L_{\rm canon} = 0$. This simplified expression is particularly useful because it is linear in radius except for field nonlinearities, and is particularly amenable to analytic solutions.

For a sinusoidally varying magnetic field, we can use a dimensionless length scale $\tau = \pi z/L$, in which case the radial equation takes the form of the Mathieu equation

$$\ddot{r} + [a - 2q\cos(2\tau)]r = 0,$$

with $a = 2q$ and

$$q = \left(\frac{qB_{\max}L}{4\pi P_z}\right)^2 = \left(\frac{3\chi}{40\pi}\right)^2.$$

The first two regions of stability for the Mathieu equation under the restriction that $a = 2q$ correspond to the following values of χ:

$$\chi < 24.04, \qquad\qquad 39.54 < \chi < 57.14,$$

which is in good agreement with the results quoted above. The first resonance value quoted above, at $\chi \simeq 23.9$, was in fact too conservative because the swings in beta function near resonance can be quite large and gave a misleading indication about the ultimate stability of the motion.

8. Extension of Simplified Geometries – Fourier Components and Lattice Types

Here we take a further look at extended solenoids, expressing the magnetic field on axis in terms of Fourier components. It is problematic to maintain the analogy with the thin lens case, so instead we continue to use the quantity

$$\chi \equiv \frac{B_{\max}[\mathrm{T}]\ L[\mathrm{m}]}{P_z[\mathrm{GeV/c}]},$$

and we assume a charge of e throughout. The quantity ξ defined for thin lenses scales like $\chi^2\ell/L$. The periodicity of the magnetic field is kept at $2L$, and the lattice is divided into cells of length L which are similar except that the magnetic field may reverse itself from one cell to the next.

We first consider two general sets of idealized magnetic field geometries, obtained by adding either a second or a third harmonic to an underlying sinusoidally varying magnetic field. We show a "phase diagram" of the regions of bounded motion as determined by the relative magnitude of the second harmonic. The two magnetic field models are

$$B_z(z) = B_1 \sin\left(\frac{2\pi z}{L}\right) + B_2 \sin\left(\frac{4\pi z}{L}\right),$$

and

$$B_z(z) = B_1 \sin\left(\frac{\pi z}{L}\right) + B_3 \sin\left(\frac{3\pi z}{L}\right).$$

Note that the addition of a second harmonic destroys the symmetry between positive and negative field regions, and requires a cell length L which is twice the definition taken above for a FOFO lattice. This artificially doubles the lattice parameter χ, just as in the thin lens analysis changing the periodicity doubled the parameter ξ.

In Figures 10 and 11, a picture of the boundaries between bounded and unbounded motion is shown, and lattice types having different qualitative behavior are labelled according to the conventions in previous publications [5]. Concrete examples of the AltSol, SFOFO, and RFOFO lattices are considered below. It is interesting to note the smooth transition between the AltSol and SFOFO cases; the intermediate region has a vanishingly small region of instability and roughly corresponds to the case where the beta function drops to a minimum at both zero and non-zero values of the magnetic field. Qualitatively, the shape of the beta function resembles that of a FOFO lattice, and both the large momentum acceptance and relatively large minimum beta function mimic the behavior of a FOFO lattice. As the magnetic field component B_3 is increased, the minimum at low field decreases and the minimum at high field increases, leading to an SFOFO type of lattice. If B_3 is decreased, the magnetic field becomes more peaked, and the local minima of the beta function move in the opposite direction, leading to an AltSol type of lattice. In either case, the minimum beta achieved becomes smaller as the magnetic field geometry is deformed away from the intermediate case. The choice of which way to alter the field in a given lattice will probably be determined by engineering considerations.

We now consider in detail three examples of lattices designed for minimizing the beta function. A magnetic field created by current sheets has been used for single particle tracking,

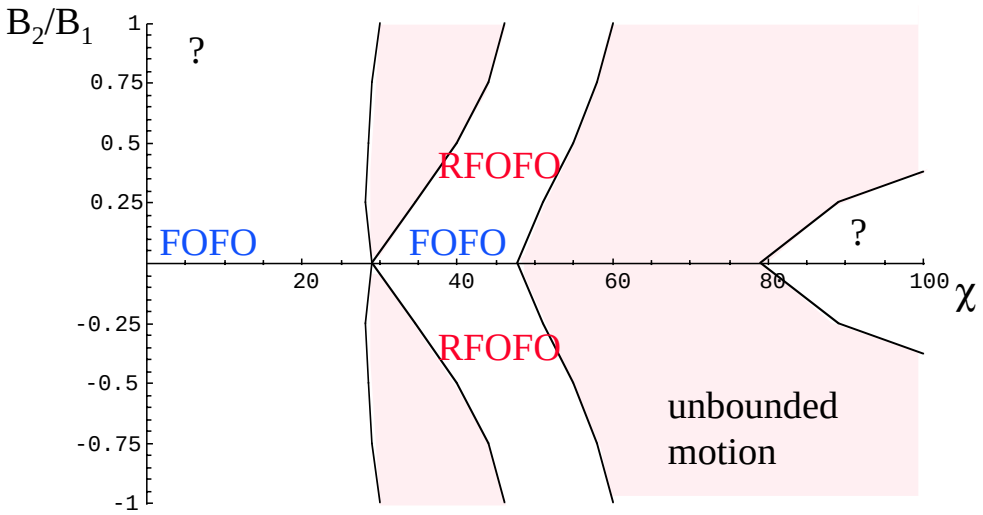

Figure 10: Phase diagram for lattice behavior when the second harmonic is added to a sinusoidal magnetic field. The lattice behavior with momentum, parametrized by $\chi = B_{\max}[\mathrm{T}]L[\mathrm{m}]/P_z[\mathrm{GeV/c}]$, is indicated as a function of B_2/B_1, the ratio of the two Fourier components of the axial magnetic field.

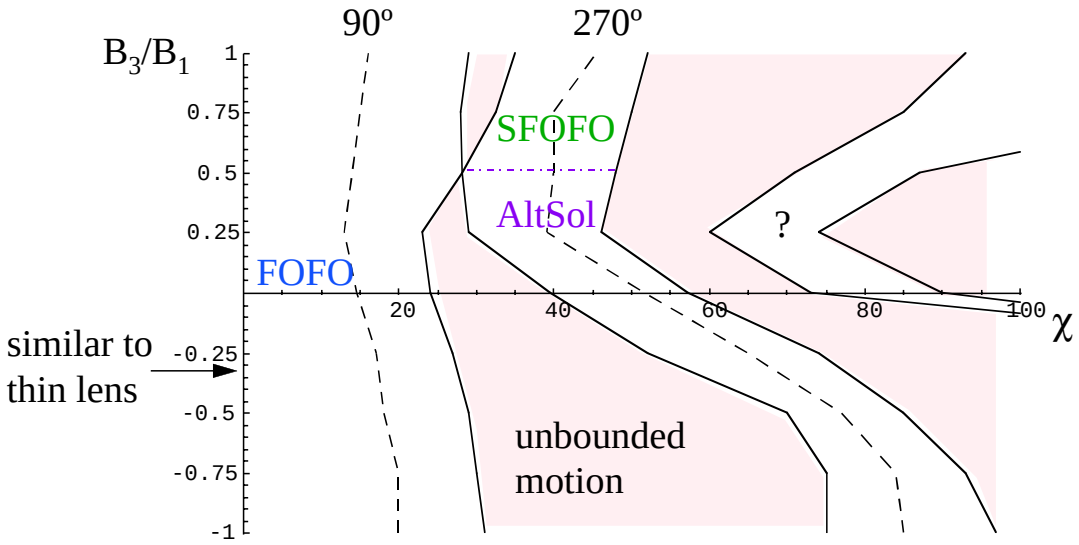

Figure 11: Phase diagram for lattice behavior when the third harmonic is added to a sinusoidal magnetic field. The lattice behavior with momentum, parametrized by $\chi = B_{\max}[\mathrm{T}]L[\mathrm{m}]/P_z[\mathrm{GeV/c}]$, is indicated as a function of B_3/B_1, the ratio of the two Fourier components of the axial magnetic field.

and the resulting magnetic field on axis has been roughly matched to a Fourier decomposition using up to three harmonics. Each example corresponds to one of the basic types of lattice in the second stability region.

The first, which is an "alternating solenoid" type (denoted AltSol), has the minimum beta in a region of high magnetic field and cannot be equated with a thin lens model. The second two models are similar to the bi-periodic thin lens systems examined in Section 5; these will both be referred to as Super-FOFO lattices because of the additional periodicity. The first, denoted SFOFO, has both even and odd symmetry points in the axial field, and the other, denoted RFOFO, has only odd symmetry points. These particular examples are comparable to each other and they both approximate the configurations as listed in [6]. These lattices correspond to extended versions of the doubly-periodic thin lens systems, with the possibility of bucking coils being added in the gaps between solenoid pairs to reduce the fringe fields. The RFOFO design is less likely to require bucking coils and so can more easily be designed for high peak magnetic fields.

AltSol:

First, we consider an "alternating solenoid" example, which is close to a simple sinusoid. The FOFO lattice has been described in detail in Section 7. Given the small bore size of the magnets compared to the periodicity in the coil geometry shown below, the magnetic field on axis is not purely sinusoidal but has a more square profile. An approximation to this magnetic field is

$$B_z(z) \simeq \frac{B_{\max}}{0.972}\left[\sin\left(\frac{\pi z}{L}\right) + 0.03\sin\left(\frac{3\pi z}{L}\right) - 0.12\sin\left(\frac{5\pi z}{L}\right)\right].$$

There is only one region of maximum magnetic field in each cell, which is also where the minimum beta occurs.

There are two regions of acceptance which we consider. The first corresponds to a FOFO type region and is given by

$$0 < \chi \lesssim 23.5,$$

although there is a harmonic resonance in the betatron tune, corresponding to 90 degree phase advance per cell, at $\chi \simeq 14.0$, as well as other resonances. There is also a second region of stability at lower momenta in the range $36.3 \lesssim \chi \lesssim 51.4$.

In the second region of stability the momentum range $\Delta P/P$, which is the momentum acceptance as defined above, has the value

$$\frac{\Delta P}{P} \simeq 0.17.$$

This is smaller than the typical value of 0.24 used in FOFO channels. However, at $\chi \simeq 42.6$, which is at the center of the momentum acceptance region, the minimum $\beta_\perp$ is given by

$$\beta_{\rm M} \simeq 0.061\ L,$$

which is much smaller than what can be achieved in the "FOFO" region for the same momentum acceptance. For these narrow bands of momentum acceptance, the minimum

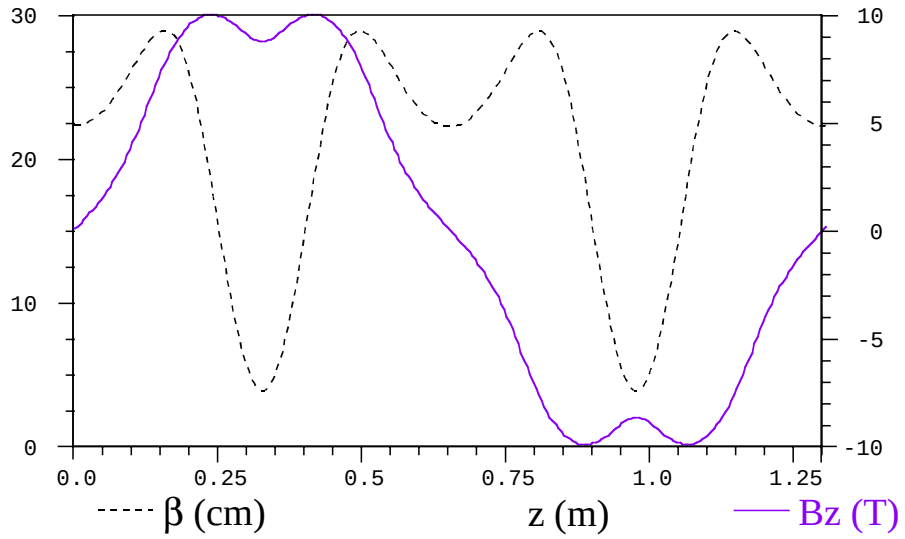

Figure 12: AltSol example, plot of magnetic field on axis, and of matched $\beta_\perp$ for a beam with no net canonical momentum.

beta at the center of the momentum range is practically equivalent to the definition of $\beta_{\rm M}$ used in Section 5.

In Figure 12, the magnetic field is shown for a lattice with $L = 0.65$ m, and $B_{\rm max} \simeq 9.96$ T, for which the central momentum is $P_0 \simeq 150$ MeV/c. The beta function as calculated by a moments code [3] is indicated. The minimum beta for $P_z = P_0$ is roughly 3.8 cm, and the allowed range of momenta is 125 MeV/c $\lesssim P_z \lesssim$ 175 MeV/c, which represents a momentum acceptance of $\pm 17\%$. This corresponds to $\beta_{\rm M} \simeq 0.058\ L$ and $37.1 \lesssim \chi \lesssim 52.1$, which is a reasonable match with the results using Fourier components for the magnetic field. All figures are for systems defined by simple coil configurations rather than the idealized description of the magnetic fields on axis in terms of Fourier components. A sketch of the coil configuration used for these results is given in Figure 13.

SFOFO:

The magnetic field on axis is approximately

$$B_z(z) \simeq \frac{B_{\rm max}}{1.7}\left[\sin\left(\frac{\pi z}{L}\right) + 1.1\sin\left(\frac{3\pi z}{L}\right) + 0.2\sin\left(\frac{5\pi z}{L}\right)\right].$$

The maxima of the magnetic field are separated by $L/3$. There are two regions of acceptance which we consider. The one corresponding to Region I in the thin lens analysis is given by

$$0 < \chi \lesssim 28.5,$$

although there is a harmonic resonance in the betatron tune at $\chi \simeq 16.5$. There is also a region of momentum acceptance at low momenta corresponding to Region II, $38.8 \lesssim \chi \lesssim 54.5$.

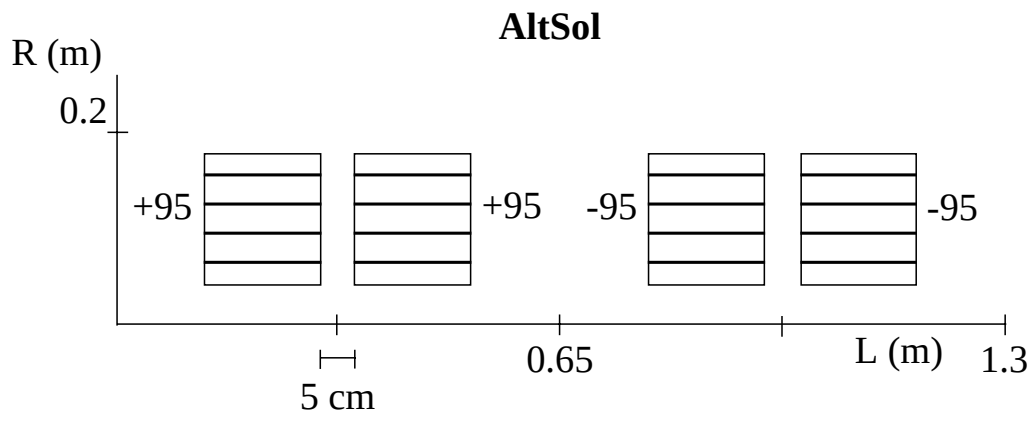

Figure 13: Coil configuration corresponding to AltSol geometry. Numbers correspond to current density, each solenoid is modelled with 4 current sheets, with 2.85×10^6 A/m for each current sheet. Each solenoid is 17 cm long and 12 cm thick, with a 10 cm diameter bore. The cell length is 0.65 m, and the peak field on axis is 9.96 T. There is a 5 cm gap between adjacent pairs of solenoids.

It is difficult to compare directly between cases because the region of high magnetic field is more localized in the Super-FOFO cases. We already have a strong contrast to the thin lens case, however; the range $\Delta P/P$, which is the momentum acceptance as defined above, has the value

$$\frac{\Delta P}{P} \simeq 0.17,$$

while for the thin lens case $\Delta P/P \lesssim 0.17$ even for the case of barely broken symmetry. At $\chi \simeq 45.3$, which is at the center of the momentum acceptance region, the minimum $\beta_\perp$ is given by

$$\beta_{\rm M} \simeq 0.071\ L.$$

In Figure 14, the magnetic field is shown for a lattice with $L = 0.50$ m, and $B_{\rm max} \simeq 10.75$ T, for which the central momentum is $P_0 \simeq 120$ MeV/c. The beta function as calculated by a moments code [3] is indicated. The minimum beta for $P_z = P_0$ is roughly 3.7 cm, and the momentum acceptance is $\pm 17\%$, with an allowed range of momenta 100 MeV/c $\lesssim P_z \lesssim$ 140 MeV/c. This corresponds to $\beta_{\rm M} \simeq 0.074\ L$ and $38.4 \lesssim \chi \lesssim 53.8$, which is a reasonable match with the results using Fourier components for the magnetic field. A sketch of the coil configuration used for these results is given in Figure 15.

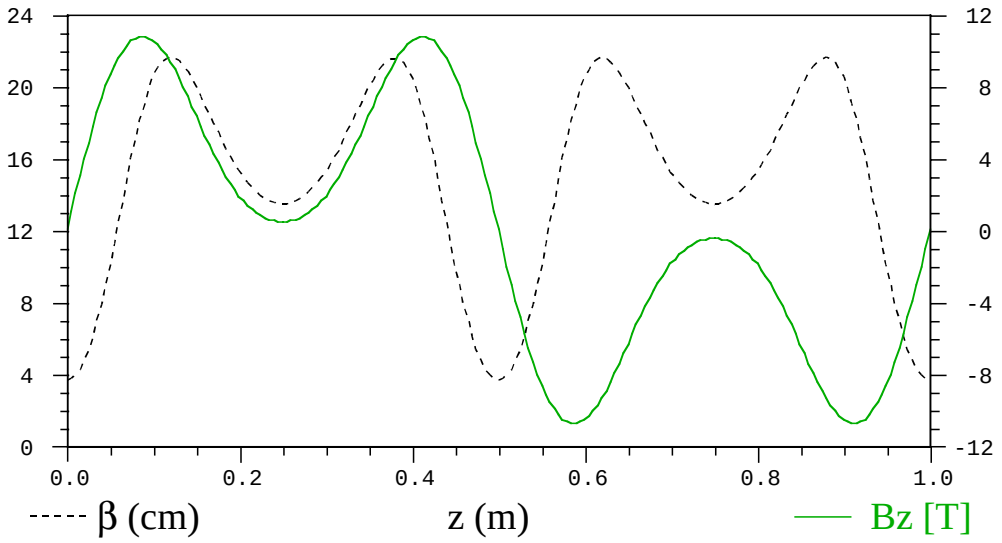

Figure 14: SFOFO example, plot of magnetic field on axis, and of matched $\beta_\perp$ for a beam with no net canonical momentum.

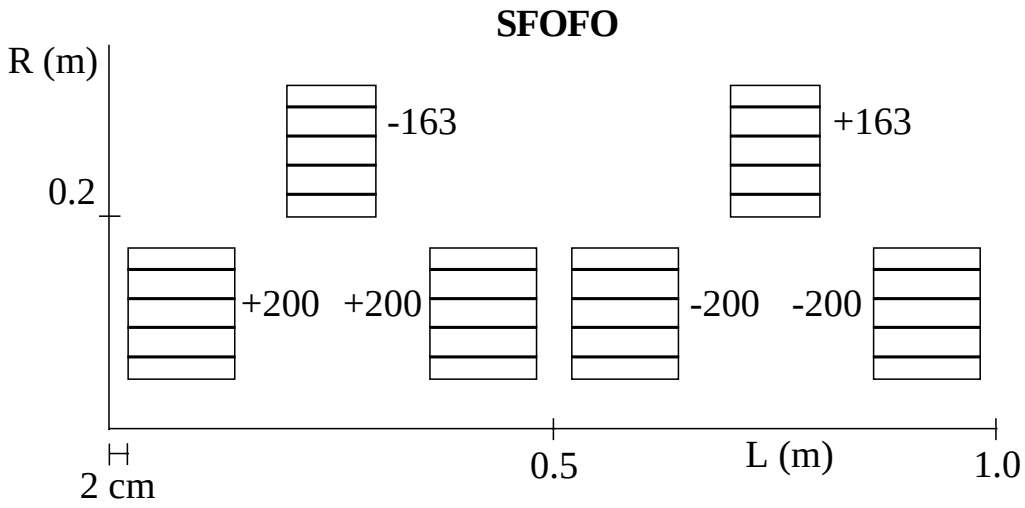

Figure 15: Coil configuration corresponding to SFOFO geometry. Numbers correspond to average current density; each solenoid is modelled with 4 current sheets. Large solenoid: 12 cm long and 12 cm thick with a 10 cm diameter bore, and 6.0×10^6 A/m for each current sheet. Small solenoid: 10 cm long and 12 cm thick with a 40 cm diameter bore, and 4.9×10^6 A/m for each current sheet. The cell length is 0.50 m, and the peak field on axis is 10.75 T. There is a 4 cm gap between adjacent pairs of large solenoids.

RFOFO:

The magnetic field on axis is approximately

$$B_z(z) \simeq \frac{B_{\max}}{1.213}\left[\sin\left(\frac{2\pi z}{L}\right) + 0.4\sin\left(\frac{4\pi z}{L}\right) + 0.05\sin\left(\frac{6\pi z}{L}\right)\right].$$

For comparison with SFOFO, we define L to be the length of a unit cell, which repeats itself without reversing the magnetic field, unlike the other two examples. The maxima of the magnetic field are separated by about 0.33 L. There are two regions of acceptance which we consider. The one corresponding to Region I is given by

$$0 < \chi \lesssim 28.4.$$

Because the symmetry is already broken, the case of 90 degree phase advance per cell is less significant. There is also a region of momentum acceptance at low momenta corresponding to Region II, $38.6 \lesssim \chi \lesssim 54.4$. The range $\Delta P/P$ is

$$\frac{\Delta P}{P} \simeq 0.17,$$

which is smaller than in SFOFO. At $\chi \simeq 45.2$, which is at the center of the momentum acceptance region, the minimum $\beta_\perp$ is given by

$$\beta_{\rm M} \simeq 0.070\ L.$$

In Figure 16, the magnetic field is shown for a lattice with $L = 0.55$ m, and $B_{\max} \simeq 9.84$ T, for which the central momentum is $P_0 \simeq 120$ MeV/c. The beta function as calculated by a moments code [3] is indicated. The minimum beta for $P_z = P_0$ is roughly 3.9 cm, and the momentum acceptance is $\pm 17\%$, with an allowed range of momenta 100 MeV/c $\lesssim P_z \lesssim$ 140 MeV/c. This corresponds to $\beta_{\rm M} \simeq 0.071\ L$ and $38.6 \lesssim \chi \lesssim 54.3$, which is a reasonable match with the results using Fourier components for the magnetic field. Note that compared with the SFOFO design, the cell length was stretched by 5 cm, while the small gap between magnets was kept constant. A sketch of the coil configuration used for these results is given in Figure 17.

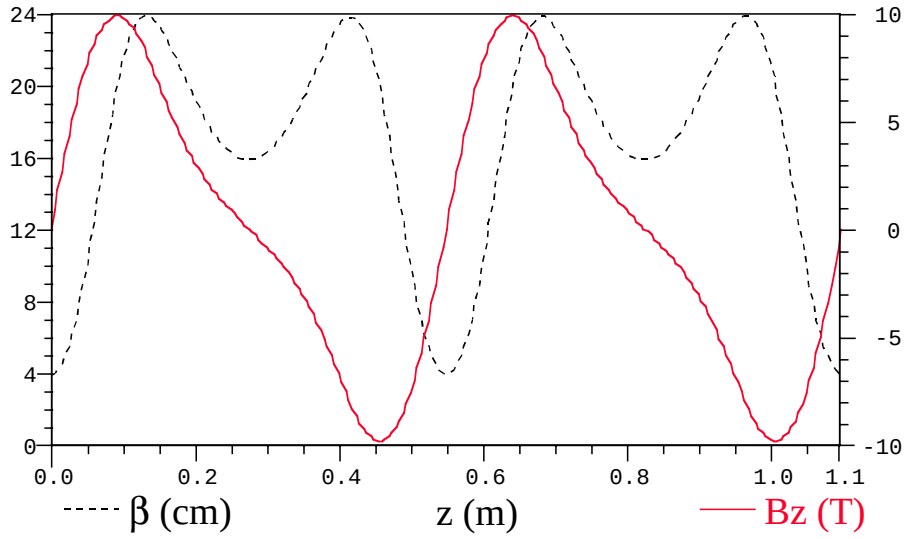

Figure 16: RFOFO example, plot of magnetic field on axis, and of matched $\beta_\perp$ for a beam with no net canonical momentum.

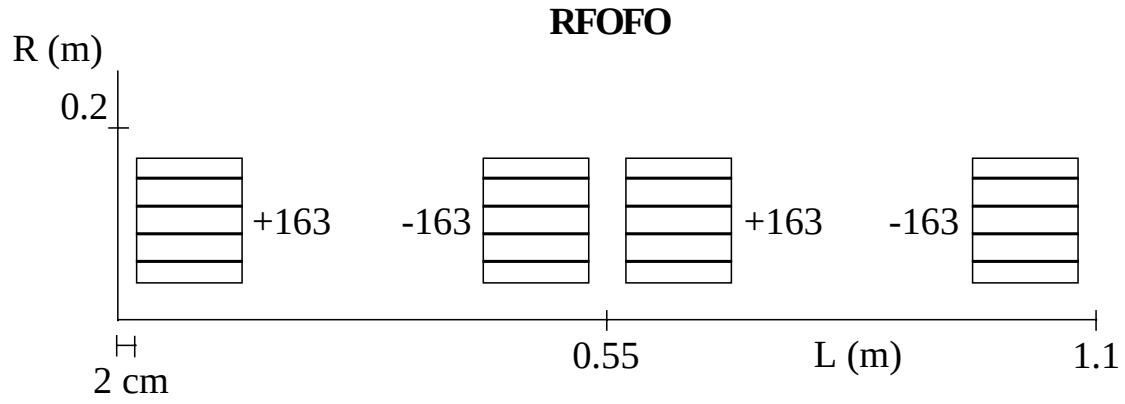

Figure 17: Coil configuration corresponding to RFOFO geometry. Numbers correspond to average current density; each solenoid is modelled with 4 current sheets, with 4.90 $\times 10^6$ A/m for each current sheet. Solenoids are 12 cm long and 12 cm thick, with a 10 cm diameter bore. The cell length is 0.55 m, and the peak field on axis is 9.84 T. There is a 4 cm gap between adjacent pairs of solenoids.

Summary:

These cases all are chosen to have roughly similar minimum beta function and momentum acceptance. We see that the required current density to propagate the same momentum beam is significantly less for the RFOFO lattice than for the SFOFO. The AltSol case requires even less current density, and furthermore can propagate a higher momentum beam for the same peak magnetic field.

As a quality factor for describing these results, consider

$$Q_c \equiv \frac{L}{\beta_{\rm M}} \left(\frac{\Delta P}{P}\right)^2 .$$

For a thin lens, Q_c varies in the range 0.12 and 0.25, with the lower values only for d/L close to 1/2. The beta functions found for the examples considered here correspond loosely to $d \simeq 0.4\ L$. For SFOFO, we have $Q_c \simeq 0.39$, and for RFOFO, $Q_c \simeq 0.41$, which indicates that the allowed range of momenta is about 30% wider than expected from thin lens calculations. For a purely sinusoidal magnetic field, the second stability region has a quality factor $Q_c \simeq 0.54$, while for the realistic AltSol case $Q_c \simeq 0.49$. Note that this quality factor does not describe the relative difficulty in producing the different lattice geometries. The better energy acceptance for these cases is important for achieving cooling goals. The smooth variation in the magnetic field helps to propagate off-momentum particles. This suggests a positive role for the fringe fields of magnets, although the shaping of the magnetic field can also be achieved through a variation in current density in a magnet with small aperture. Because these lattices depend upon rapidly varying the magnetic field, it would be advantageous to design coils that produce this geometry without "wasting" as much current through cancellations of the magnetic field produced by opposing magnets.

9. Coupling to Longitudinal Motion: Amplitude Correlation

In considering nonlinear effects, an important source of coupling is the correlation between energy and transverse amplitude in a bunched beam. This correlation comes about because the average forward velocity of a particle is given by

$$\bar{v}_z \simeq v\left[1 - \frac{1}{4}(A_1^2 + A_2^2)\bar{\gamma}_p + \frac{L_{\rm canon}}{P_z}\bar{\kappa}\right], \tag{26}$$

where $\bar{x}$ is the average of the quantity x for a single particle over many betatron oscillations. The resulting spread in velocities leads to different E_z from an RF system being experienced by particles that start out in the same longitudinal phase space. There is also a correlation with canonical angular momentum unless the magnetic field repeatedly reverses direction. For a spinning beam, this varies even for particles having the same total amplitude $A_\perp^2$ as defined above. Thus, in the presence of RF nonlinear effects, in particular coupling between the transverse and longitudinal motion, can cause a beam to separate into a complicated function interrelating $A_1^2 + A_2^2$, $L_{\rm canon}$, and longitudinal amplitude. Thus the beam envelope model used above should be further generalized to a full 6D model to describe a bunched beam with net canonical momentum. However, the above expressions are convenient as a relatively simple set of equations for the beam, and usually we consider beams with a small value of $\mathcal{L}$.

Now we consider the form of the RF bucket, and the distribution in longitudinal phase space once the amplitude correlation has been taken into account. For simplicity, we consider a lattice with $\bar{\kappa} = 0$ and a beam with $\mathcal{L} = 0$, so there are no canonical momentum correlations. Neglecting transit time effects and smoothing out the forces, the RF system can be roughly modelled as a time-varying potential. Letting t be the time relative to a reference particle for crossing at a fixed position, the equations of motion in an RF simplify to:

$$E' = \bar{\mathcal{E}}\left[\sin(\omega t + \phi) - \sin\phi\right]$$
$$t' = \left\langle \frac{1}{v_z} \right\rangle - \frac{1}{v_R},$$

where $\bar{\mathcal{E}}$ is the average peak gradient of the RF and v_R is the velocity of the reference particle. The reference phase ϕ here counteracts the energy loss in the absorber. Treating the amplitude effect as a small term, we approximate the time equation as

$$t' \simeq \frac{1}{v} - \frac{1}{v_A}$$

with

$$v_A = v_R\left(1 + \frac{1}{4}\bar{\gamma}_p A^2\right);$$

here, $A^2 \equiv A_1^2 + A_2^2$ and

$$\bar{\gamma}_p = \frac{1}{L}\oint\left(1 + \alpha_p^2 + \beta_p^2\kappa^2\right)\frac{dz}{\beta_p(z)},$$

L is the length per cell, and the integral is taken over a single cell. The focussing strength along the lattice is

$$\kappa(z) = \frac{qB_z(z)}{2P_z}.$$

Then the equation of motion can be written in terms of a Hamiltonian

$$U = \frac{E - E_A}{v_A} - (P - P_A) - \frac{\bar{\mathcal{E}}}{\omega}\left[\cos(\omega t + \phi) - \cos\phi + \omega t \sin\phi\right].$$

For a given amplitude, the RF bucket is centered about an energy above the reference energy, given by

$$E_A \simeq E_R\left[1 + \frac{1}{4}\bar{\gamma_p}A^2\left(\frac{P_R}{mc}\right)^2\right].$$

From this point we consider the use of E_A as sufficient to incorporate the amplitude dependence in the longitudinal distribution. However, the RF bucket is not a simple harmonic well so the bucket will be distorted. Expanding to third order in $E - E_A$ and in t,

$$U \simeq \frac{1}{2}\frac{m^2}{P_A^3}(E - E_A)^2\left(1 - \frac{E - E_A}{v_A P_A}\right) + \frac{1}{2}\bar{\mathcal{E}}\omega t^2\cos\phi\left(1 - \frac{1}{3}\omega t\tan\phi\right),$$

so the RF bucket is asymmetric in both energy and time. Taking into account the distortion in energy arising from the fact that the distribution is Gaussian in P_z, the energy distribution is roughly matched when

$$P_0 \simeq P_R\left(1 + \frac{c^2\sigma_P^2}{2E_R^2}\right).$$

Similarly, the time should be shifted by roughly

$$t_0 \simeq \frac{1}{6}\omega\sigma_t^2\tan\phi.$$

These are only rough estimates, in particular choosing a different criterion for fitting the Gaussian beam could change this value by as much as a factor of 2. A calculation of the higher order correlations and their evolution, or simply trial and error, would yield more definitive results.

We proceed to consider transversely matched beams in geometries where the magnetic field periodically reverses sign. Over many cells and many betatron periods, the average forward velocity of a particle is independent of its initial betatron phase unless there is a resonance between the betatron period and the lattice spacing. Then the forward velocity satisfies

$$\left\langle\frac{v^2}{v_z^2}\right\rangle = 1 + \langle(x')^2\rangle + \langle(y')^2\rangle \simeq \left(1 + \frac{1}{2}A^2\bar{\gamma_p}\right),$$

For beams which are far from resonance,

$$\bar{\gamma_p} \simeq \frac{2}{\beta_p} \simeq \frac{P_z}{q\langle B_z^2\rangle^{1/2}}.$$

Note that γ_p satisfies

$$\gamma_p' = \beta_p(\kappa^2)',$$

so it is always changing in the same way as the magnitude of the magnetic field.

In an ideal FOFO lattice, a close approximation to $\bar{\gamma_p}$ is

$$\bar{\gamma_p} \simeq \frac{2}{\beta_{\rm min}} \left[1 + \frac{1}{2}\left(\frac{P_{\rm cr}}{P_z}\right)^3\right]^{-1},$$

where

$$\frac{P_{\rm cr}}{P_z} \simeq \frac{B[\mathrm{T}]\ L[\mathrm{m}]}{23.9\ P_z[\mathrm{GeV/c}]}.$$

Note that for a FOFO lattice the cell length L is defined to be the distance between zeroes of the magnetic field.

For the Super-FOFO lattices described in Section 8, by comparison, $\bar{\gamma_p}$ falls in the range

$$\frac{0.75}{\beta_{\rm min}} \lesssim \bar{\gamma_p} \lesssim \frac{0.85}{\beta_{\rm min}}.$$

A larger $\bar{\gamma_p}$ indicates a stronger correlation, which depends on the type of lattice and the actual value of $\beta_{\rm min}$.

When $\epsilon_\perp \ll \beta_p$, so the transverse angles are small, we can approximate

$$\langle v_z \rangle \simeq v\left(1 - \frac{1}{4}\bar{\gamma_p}A^2\right).$$

To have a given forward velocity v_R, corresponding to a zero-amplitude particle with energy E_R, a particle must have energy

$$E_A \simeq E_R\left(1 + \frac{1}{4}\bar{\gamma_p}A^2\frac{P_R^2}{m^2c^2}\right).$$

For an RF system which drives synchrotron oscillations that are much longer than the cell length, so the betatron oscillations have a chance to average out, a matched beam can only have its longitudinal distribution depend on E, t, and A^2, where t is the time relative to a reference particle for reaching a fixed position. In particular, there should be no dependence on betatron phase. A very rough condition for this regime is $\epsilon_\perp < \sigma_z$.

The distribution function generated by ICOOL, however, is expressed in terms of momentum so that there is normally a dependence of betatron phase in the distribution function. With carefully chosen correlations, however, a distribution with the appropriate properties can be generated. The forward momentum has the form

$$P_z = P_0 + \delta P + P_2\left[\frac{x^2+y^2}{b^2} + \frac{P_x^2+P_y^2}{(P_0+\delta P)^2}\right],$$

where P_0, P_2, and b are fixed parameters and δP is a random value having a Gaussian distribution with standard deviation σ_P. We assume the distribution is created with $\alpha_\perp = 0$ and $\mathcal{L} = 0$ (no net angular canonical momentum). The energy satisfies

$$E^2 = m^2c^4 + c^2(P_x^2 + P_y^2 + P_z^2),$$

which can be made roughly independent of betatron phase if we set

$$b \simeq \beta_\perp \left(1 + \frac{P_0}{2P_2}\right)^{-1/2}.$$

Then, neglecting terms of order A^4 and $A^2\delta P$, the energy is approximately

$$E^2 \simeq m^2c^4 + c^2(P_0 + \delta P)^2 + c^2 P_0 \left(P_0 + 2P_2\right) \frac{A^2}{\beta_\perp}.$$

This has the correct dependence on amplitude if

$$P_2 \simeq P_0 \left(\frac{\beta_\perp \bar{\gamma_p} \gamma_R^2}{4} - \frac{1}{2}\right).$$

For the case where $\bar{\gamma_p} \simeq 2/\beta_{\rm min}$, this simplifies to

$$P_2 \simeq \frac{P_0^3}{2m^2c^2}, \qquad b \simeq \beta_\perp \frac{v_R}{c}.$$

If the beam is not matched, there will be two main effects on the correlation: the amplitude correlation will undergo synchrotron oscillations about the matched value, and there will be betatron oscillations of the correlation between betatron phase and energy. There will always be some jitter because the initial forward velocity is different from the average velocity, especially when the synchrotron tune approaches a harmonic.

10. Conclusions

A paraxial theory for beam envelope equations in solenoidal fields has been developed, and applied towards lattices designed for ionization cooling of muons. This theory is similar in form to the Courant-Snyder formalism for quadrupole focussing systems. The effect of material in the channel does lead to significant changes in transverse emittance, but is otherwise a small perturbation so long as build-up of canonical angular momentum is avoided and the average energy loss is recovered by RF acceleration.

Because thin lens systems do not adequately describe the magnetic field configuration in realistic cooling channels, systems of extended solenoid magnets, typically with significant fringe fields, have been modeled in terms of a Fourier decomposition of the magnetic field on axis. This leads to a good prediction of lattice parameters required to propagate a beam, and of the resulting beta function. In addition, the four basic lattice types so far considered, FOFO, AltSol, and the two Super-FOFO channels, have all been modelled and put into the context of this analysis. Trade-offs between the minimum beta function and momentum acceptance have been characterized by a quality factor, $Q_c \equiv (\Delta P/P)^2 L/\beta_{\rm min}$, where $\beta_{\rm min}$ is evaluated for the central value of the momentum range for stable motion within the lattice. This quality factor ranges from below 0.25 for thin lens systems, to roughly 0.5 for realistic extended systems.

In addition, without incorporating feedback between longitudinal and transverse phase space, the longitudinal behavior of a finite emittance beam can be evaluated in two limiting cases: where the beam is unbunched, in which case the average velocity as a function of P_z and amplitude is known; and for a well bunched beam, where correlations between energy and amplitude for a matched beam were shown. The evolution of these correlations can also be used to describe poorly matched beams, or for designing transition regions connecting different lattices.

References:

1. M. Reiser, Theory and Design of Charged Particle Beams, John Wiley & Sons, NY, 1994.
2. As used in the ICOOL code; see also G.R. Lynch and O.I. Dahl, Nucl. Instrum. Methods **B58**, 6 (1991).
3. Unnamed moments code by B.A. Shadwick.
4. R.C. Fernow, Muon Collider Note 26.
5. See, for example, Muon Collider Notes 11, 23 and 36.
6. Muon Collider Notes 36 and 45.